ISSN 0021-3640, JETP Letters, 2015, Vol. 102, No. 3, pp. 176–183. © Pleiades Publishing, Inc., 2015.
Original Russian Text © O.A. Dubovsky, V.A. Semenov, A.V. Orlov, 2015, published in Pis'ma v Zhurnal Eksperimental'noi i Teoreticheckoi Fiziki, 2015, Vol. 102, No. 3, pp. 202–210.

Gyrosolitons and Helical Surfing Diffusion of Impurity Atoms in Reactor Fuel Materials

O. A. Dubovsky, V. A. Semenov, and A. V. Orlov
Leipunsky Institute of Physics and Power Engineering,
pl. Bondarenko 1, Obninsk, Kaluga region, 249033 Russia
e-mail: orlovav@obninsk.ru

Received April 1, 2015; in final form, June 30, 2015

Fundamentally new gyrosolitons with helical trajectories of motion have been revealed in UO_2 and PuO_2 reactor fuel materials by the computer simulation of the microdynamics of high-amplitude atomic vibrations. The phonon spectra of nanostructures, as well as of gyrotropic materials, include quasioptical branches with different-sign linear dispersion. The corresponding branches of gyrosolitons have been revealed on the phase plane in the spectral density of vibrations. The main dynamic event of the kinetic process of helical surfing diffusion of impurity atoms on gyrosolitons has been observed.

DOI: 10.1134/S0021364015150023

The microdynamics of high-amplitude nonlinear vibrations of crystal lattices of U, UN, UO_2, and PuO_2 fuel materials at high temperatures is now experimentally studied by the neutron spectrometry method. The authors of [1] revealed a new resonance peak in the spectra of scattering of neutrons from the α phase of uranium at a high temperature (500 K), which was not observed at lower temperatures, and attributed it to the generation of a nonlinear self-localized mode. It was shown in [2] that a dynamic multisoliton superlattice could be generated in crystals at a high energy. The splitting of an optical branch, which is caused by the generation of a superlattice, was revealed in [3] in the spectra of scattering of neutrons from a NaI crystal at the reconstruction of vibrations of the crystal with reference to [2]. Promising UO_2 dioxide fabricated using nanotechnology was presented in [4]. At the Joint Institute for Nuclear Research, on the DIN-2PI neutron spectrometer, at high temperatures (up to 1500 K), spectra of the scattering of neutrons from reactor fuel materials are measured and spectra of vibrations of their crystal lattices are reconstructed to determine the necessary thermodynamic characteristics of the materials [5, 6].

The theory of nonlinear acoustic and infrared optical vibrations of crystals [7–11], as well as neutron and optical experiments, showed that the nonlinearity of vibrations, which is incompletely taken into account in the quantum theory, is responsible not only for phonon–phonon scattering in an ensemble of dissociated multiphonon states but also for the appearance of fundamentally new bound multiphonon states. These are bound biphonons, triphonons, quartaphonons, and pentaphonons in the quantum approach [8–11] and various nonlinear waves (solitons, breathers, etc. [12]). Triphonons [9] were observed more recently experimentally [13] in the spectra of scattering of neutrons by titanium hydride. New types of nonlinear waves were recently revealed: undulator solitons determining the microdynamics of structural phase transitions [14] and bisolitons with weak [15] and strong [16] coupling between solitons. Genetically close gyration effects of rotation of the plane of polarization of the electromagnetic radiation of excitons in gyrotropic materials were presented in [17]. Surface waves at the boundary between contacting enantiomorphic gyrotropic materials were studied phenomenologically in [18, 19] and microscopically in [20].

Figure 1a shows the general 3D structure of arrangement of (closed circles) uranium and (open circles) oxygen atoms in the unit cube of similar UO_2 and PuO_2 crystals with an fcc lattice. One spatial diagonal with two U atoms at the corners of the cube and two O atoms nearest to U atoms is distinguished. On the periodic continuation of this diagonal, in the nearest environment of each U atom, two O atoms are located, constituting in combination a UO_2 linear “quasimolecule.” The period of the 3D crystal lattice of this $Fm3m$ group is $r = 5.47$ Å. The distance between the uranium and oxygen atoms in the quasimolecule is $a = \sqrt{3}r/4 = 2.37$ Å. A computer simulation of a nanocrystal consisting of 27 cubes that are shown in Fig. 1a and are composed into a Rubik's cube with the corresponding displacements by a lattice constant is performed. Figure 1b shows this nanocrystal in 3D space in a projection where the spatial diagonal of cubes

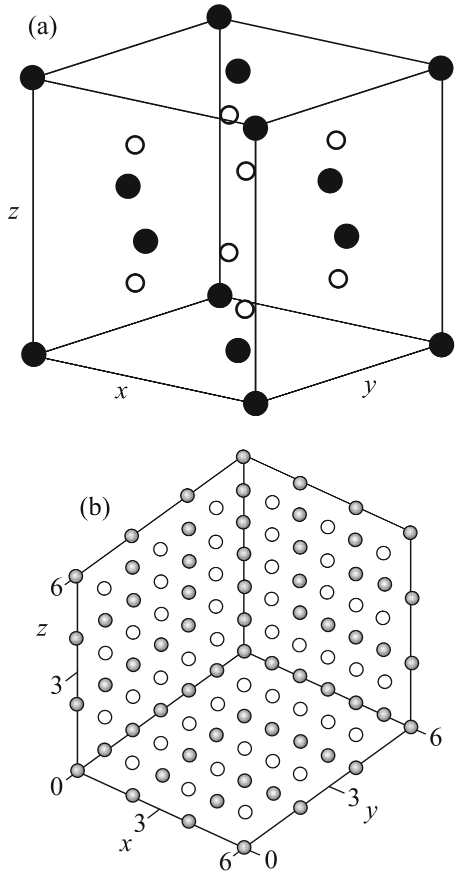

Fig. 1. Crystal structure of UO_2. (a) Unit cube with (closed circles) U and (open circles) O atoms. (b) Rubik's cube consisting of unit cubes shown in panel (a) with a spatial diagonal orthogonal to the plane of the figure.

shown in Fig. 1a is perpendicular to the plane of the figure. A standard 2D structure of hexagonal close packing of atoms with surface oxygen and uranium atoms is seen in this figure. The computer rotation of the axes shows that a 1D crystal chain of quasimolecules orthogonal to the plane of the figure is located behind each atom in Fig. 1b. The results of nanotechnological production of uranium dioxide were reported in [4]. Materials with significantly improved characteristics were obtained. For this reason, at the first stage of investigation, it is of interest to examine these characteristics for the nanocrystal, which is a constituent unit of the hexagonal close packing (Fig. 1b). This unit is represented in Fig. 2 in the form of a trigonal prism consisting of three 1D crystal chains of quasimolecules. Uranium atoms are shown by thicker points than oxygen atoms according to their masses. Study of the dynamic and spectral characteristics of such a nanocrystal is of interest because its results can be applied to more complex nanotubes, where shear and longitudinal ring solitons were observed [21]. This nanocrystal in the projection of Fig. 1b is represented as a unit triangle on the right and above the central point. Chains *1*, *2*, and *3*, which are elongated in the direction of the *x* axis in Fig. 2, in this triangle in Fig. 1b correspond to the clockwise enumeration from the central point. All atoms in the positive direction of the diagonal (the *x* axis in Fig. 2) are spaced by a distance of $(4/3)a$ from the atoms of chain *1*, and the atoms of chain *3* are spaced by the same distance of $(4/3)a$ from the atoms of chain *2*. With a further displacement of the atoms of chain *3* by the same distance of $(4/3)a$ with the transfer to edge *1* of the prism, chain *3* coincides with chain *1*. Thus, the axis of the prism is the axis of local left rotation of the third order indicated by arrows along the polygonal "helix" passing through U atoms in Fig. 2.

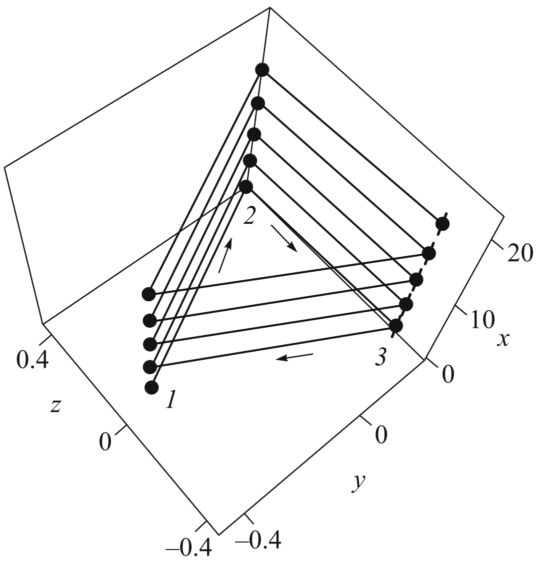

Fig. 2. Elementary hexagonal close packed nanocrystal shown in Fig. 1b consisting of 1D crystal chains *1*, *2*, and *3* shifted along a polygonal helix in the direction of arrows.

As is known, Fermi, Pasta, and Ulam [27] observed a fundamentally new return effect when studying nonlinear high-amplitude longitudinal vibrations in crystal systems consisting of 32 and 64 coupled nonlinear oscillators. Using this method, we first study the soliton microdynamics of the crystal with the number of atoms $N = 90$ and 126 presented in Fig. 2. We study longitudinal collective vibrations of atoms along the axis of the nanocrystal, i.e., in the direction of the spatial diagonal. In particular, these vibrations are responsible for the heat and mass transfer in the case of the generation of the energy on one side of the plate with the spatial diagonal orthogonal to the plane of the plate and the release of the energy on the other side.

We used the following Lennard-Jones potentials for the interaction between U and O atoms at the distance r_{UO}, between two O atoms at the distance r_{OO}, and two U atoms at the distance r_{UU}

$$
\begin{aligned}
V_{\mathrm{UO}}(r_{\mathrm{UO}}) &= (\varepsilon/12)[(a/r_{\mathrm{UO}})^{12} - 2(a/r_{\mathrm{OO}})^{6}],\\
V_{\mathrm{OO}}(r_{\mathrm{UO}}) &= (\varepsilon/12)[(2a/r_{\mathrm{OO}})^{12} - 2(2a/r_{\mathrm{OO}})^{6}], \qquad (1)\\
V_{\mathrm{UU}}(r_{\mathrm{UU}}) &= (\varepsilon/12)[(r^{(0)}_{\mathrm{UU}}/r_{\mathrm{UU}})^{12} - 2(r^{(0)}_{\mathrm{UU}}/r_{\mathrm{UU}})^{6}],
\end{aligned}
$$

where $r^{(0)}_{\mathrm{UU}} = \sqrt{\beta}a$ ($\beta = 8/3$) is the distance between the nearest U atoms in the equilibrium state. These potentials, in contrast to other potentials frequently used in the nonlinear theory of oscillations, have correct asymptotic behaviors at extremely high and extremely small interatomic distances necessary for studying high-amplitude vibrations. In Eqs. (1), the constant ε determines the energies of equilibrium bound states at which $dV(r) = dr = 0$. The experimental data from [6] are described with the value $\varepsilon = 12.5$ eV. Mobile boundary atoms at the same potentials interact with immobile "frozen" atoms of the necessary solid shell of fuel materials. The potentials were not detailed in order to avoid excess parameterization. The test introduction of different coupling constants of the same order did not change the results.

Since $\mathrm{UO_2}$ and $\mathrm{PuO_2}$ have the same crystal structure, we used the following dimensionless variables for universality: coordinates of atoms x, y, and z are presented in units of a; masses are given in units of the mass M of uranium or plutonium; and times are given in units of $t_c = \sqrt{Ma^2/\varepsilon} = 1.06^{-13}$ s, i.e., $\tau = t/t_c$. In these units, the system of dynamic equations for the coordinates of atoms has the compact general form

$$
\begin{aligned}
\frac{d^2x^{(i,\mathrm{O})}_{n,1}}{d\tau^2} &= \mu\Bigg[-\frac{\partial}{\partial x^{(i,\mathrm{O})}_{n,1}}V_{\mathrm{OO}}(x^{(i,\mathrm{O})}_{n,1} - x^{(i,\mathrm{O})}_{n-1,2})\\
&\quad - \frac{\partial}{\partial x^{(i,\mathrm{O})}_{n,1}}V_{\mathrm{UO}}(x^{(i,\mathrm{O})}_{n,1} - x^{(i,\mathrm{U})}_{n}\Bigg],\\
\frac{d^2x^{(i,\mathrm{O})}_{n,2}}{d\tau^2} &= \mu\Bigg[-\frac{\partial}{\partial x^{(i,\mathrm{O})}_{n,2}}V_{\mathrm{OO}}(x^{(i,\mathrm{O})}_{n,2} - x^{(i,\mathrm{O})}_{n+1,1})\\
&\quad - \frac{\partial}{\partial x^{(i,\mathrm{O})}_{n,1}}V_{\mathrm{UO}}(x^{(i,\mathrm{O})}_{n,1} - x^{(i,\mathrm{U})}_{n}\Bigg], \qquad (2)\\
\frac{d^2x^{(i,\mathrm{U})}_{n}}{d\tau^2} &= -\left[\sum_{j=1,2}\frac{\partial}{\partial x^{(i,\mathrm{U})}_{n}}V_{\mathrm{UO}}\left(x^{(i,\mathrm{U})}_{n} - x^{(i,\mathrm{O})}_{n,j}\right)\right]\\
&\quad - \left[\sum_{j\neq 1}\frac{\partial}{\partial x^{(i,\mathrm{U})}_{n}}V_{\mathrm{UU}}\left(x^{(i,\mathrm{U})}_{n} - x^{(i,\mathrm{U})}_{n-m(i,j)}\right)\right].
\end{aligned}
$$

Here, $x^{(i,\mathrm{O})}_{n,1}$ and $x^{(i,\mathrm{O})}_{n,2}$ are the coordinates of the "left" and "right" O atoms with respect to the coordinate $x^{(i,\mathrm{U})}_{n}$ of the central U or Pu atom in the quasimolecule, the superscript $i = 1, 2, 3$ enumerates the 1D crystal chain in Fig. 2, the superscript n is the number of the unit cell, the only nonzero matrix elements of the matrix $m(i,j)$ are $m(1, 3) = 1$ and $m(3, 1) = -1$, and $\mu = M_{\mathrm{U}}/M_{\mathrm{O}}$ is the ratio of the masses of U and O.

It is of interest to study the spectrum of low-amplitude phonon vibrations in this system. Since the unit cell of the nanocrystal contains three triatomic quasimolecules, the spectrum will include nine individual branches. When revealing fundamental features of the spectrum, the U–O and O–O interactions were disregarded at the first stage. In this case, the corresponding dispersion equation in an infinite nanocrystal (Fig. 2) with three atoms in the unit cell after the expansion in small amplitudes of vibrations for wave solutions with the wave vector k and frequency ω has the form

$$(\omega^2 - 2B)^3 - 3(\omega^2 - 2B)B^2 + 2B^3\cos(4k) = 0, \qquad (3)$$

where

$$B = 4.2\times 10^{-3}.$$

The inverse dispersion relation is directly determined from Eq. (3) in the form $k = (1/4)\arccos\{[3B^2(\omega^2 - 2B) - (\omega^2 - 2B)^3]/2B^3\}$.

Equation (3) cubic in ω^2 has the following three solutions:

$$
\begin{aligned}
\omega^{(1)}_k &= \sqrt{2B}\sqrt{1 - \cos(4k/3)},\\
\omega^{(2,3)}_k &= \sqrt{2B}\sqrt{1 + \cos[(\pi \pm 4k/3)}.
\end{aligned}
\qquad (4)
$$

Three dispersion relations (4) are shown in Fig. 3 by respective lines *1*, *2*, and *3*. It is remarkable that, in addition to the standard acoustic branch $\omega^{(1)}_k$, the spectrum includes two quasioptical branches $\omega^{(2,3)}_k$ matching at $k = 0$ with the linear dependences of the frequency on k. In this case, the group velocities $d\omega/dk$ of these branches are opposite in sign. The indicated branches are similar to optical exciton branches with the dispersion relations linear at $k = 0$ for gyrotropic optical materials, where the rotation of the polarization plane of the electric field occurs [17–20]. Taking into account the possibility of the separation of charges in $\mathrm{UO_2}$ quasimolecules, the vibrations of quasimolecules can generate quadrupole and dipole radiation [6]. The effect of spatial dispersion, which is proportional to the first spatial derivative, with the frequency linear in k is more significant in these materials than the second-order effect with the quadratic dependence of ω on k. Thus, the presence of matching branches with the linear dependence at $k = 0$ is a signature of the existence of gyrotronic excitations. The solutions of the system of nine equations including the U–O and O–O interactions gave the remaining dispersion branches in agreement with experimental data in the energy range up to 0.1 eV.

The right-hand sides of system (2) for the positions of atoms shown in Fig. 2 are identically equal to zero. To additionally test the stability of this crystal struc-

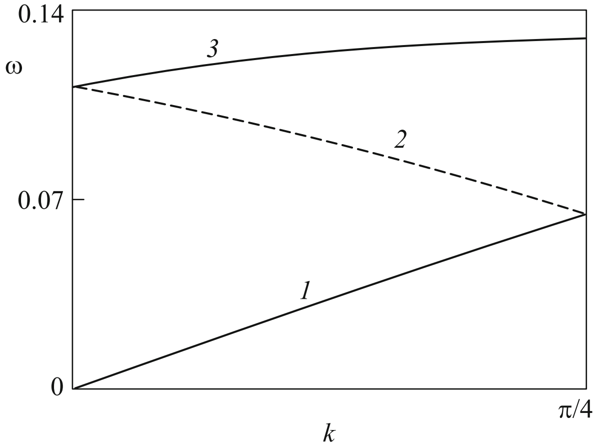

Fig. 3. Low-frequency dispersion dependences disregarding O atoms. Quasioptical branches *2* and *3* have negative and positive dispersions linear in the wave vector characteristic of gyrotropic materials.

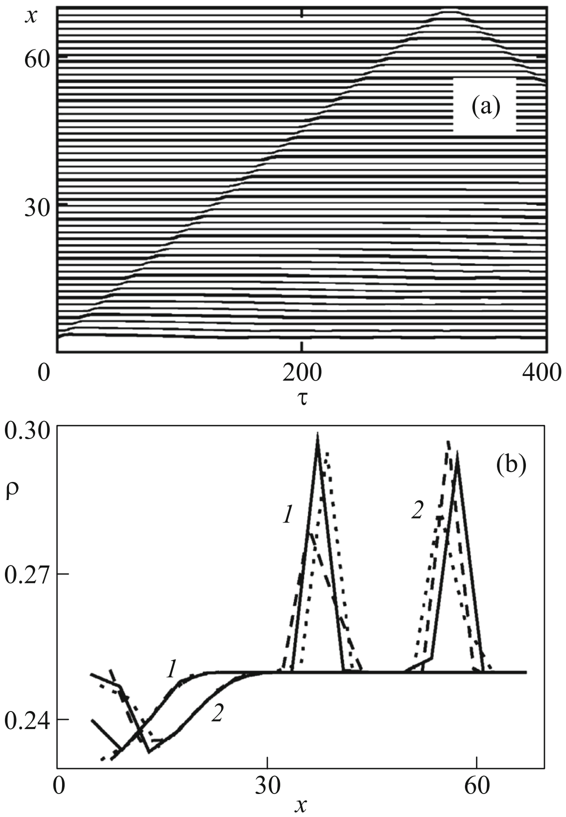

Fig. 4. (a) Time dependences of the displacement of atoms demonstrating the propagation of a gyrosoliton through U atoms disregarding O atoms. (b) Spatial distributions of the microdensity demonstrating the displacement of gyrosoliton compression density humps and rarefaction dips from *1* at $\tau = 164$ to *2* at $\tau = 252$. The solid, dotted, and dashed lines are microdensities over 1D chains *1*, *2*, and *3*, respectively.

ture, we performed the computer solution of Eqs. (2) without any initial displacements and velocities. At the first stage, to reveal the main dynamic and spectral characteristics, we considered only the system of 17 uranium atoms in the structure shown in Fig. 2 disregarding the potentials V_{OO} and V_{UO}. Figure 4a shows the time dependence of displacements of all atoms at the initial velocity of the uranium atom $v_0 = 0.1$ with the smallest initial x coordinate. It is seen that a soliton wave with a complex internal structure moves at a constant velocity $v = 0.22$ in the crystal. A weak but noticeable trace of the second excitation moving at a lower velocity is seen behind it. Details of these excitations are clarified when considering the time evolution of the spatial distribution of the microdensity $\rho_n^{(i)}(\tau) = (x_n^{(i)}(\tau) - x_{n-1}^{(i)}(\tau))^{-1}$ over the coordinate $R_n^{(i)}(\tau) = 0.5(x_n^{(i)}(\tau) + x_{n-1}^{(i)}(\tau))$ in each of the 1D chains with the number $i = 1, 2, 3$. This dependence was represented as an animation video clip. Figure 4b shows two joined frames of the video clip: at the time $\tau = 164$ with group *1* of three close dependences and at the time $\tau = 252$ with the same group *2*. The solid, dotted, and dashed lines show the microdensity in 1D chains *1*, *2*, and *3*, respectively, in each group. The fast soliton is represented by a high-density compression hump moving at the velocity $v = 0.22$ ($v = 0.4 \times 10^5$ cm/s in dimensional units). The slow soliton is represented by a rarefaction dip that moves at the velocity $v = 0.06$ and follows the compression soliton.

The video film also demonstrates the internal structure of the compression soliton. Figure 5 shows the dynamics of the internal structure of the compression soliton on a magnified scale for short time intervals. It is seen that the highest microdensity is reached on 1D chains *1*, *2*, *3*, and again *1* shown in Fig. 2 at $\tau =$ (a) 163, (b) 169, (c) 176, and (d) 182, respectively. The video clip shows how such periodic alternation occurs. Figures 5 and 4a demonstrate the motion of the compression gyrosoliton in the direction indicated by arrows in the polygonal helix in Fig. 2. The character of motion of the rarefaction gyrosoliton following the compression gyrosoliton at a lower velocity is the same.

To analyze the possibility of the generation of gyrosolitons in dioxides, we considered a system of 90 U and O atoms with the complete inclusion of the potentials V_{OO} and V_{UO}. Figure 6a shows the time dependence of the displacements of all atoms at the initial velocity of the uranium atom $v_0 = 0.05$ in chain *1* with the smallest start x coordinate. As is seen in Fig. 6a, a gyrosoliton wave with a complex internal structure moves in the crystal at the constant velocity $v = 0.19$. A trace of the second excitation moving at a lower velocity is seen behind it. Figure 6b shows two joined frames: at the time $\tau = 102$ with group *1* consisting of three close dependences and at the time $\tau = 168$ with the same group *2*. For simplicity, only microdensities of uranium atoms are shown. The system of solid, dot-

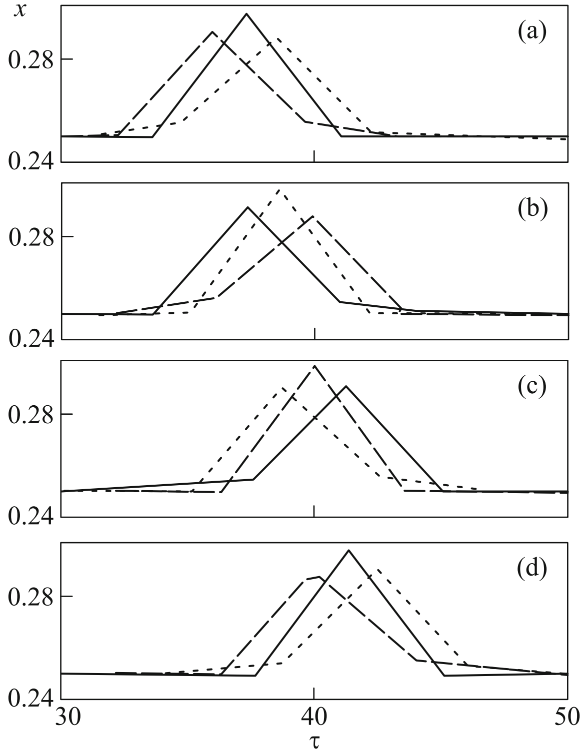

Fig. 5. Space–time dependences of the microdensity demonstrating the motion of the gyrosoliton along the helix. The maxima of the microdensity are located on (a) chain *1* at $\tau = 163$, (b) chain *2* at $\tau = 169$, (c) chain *3* at $\tau = 176$, and (d) chain *1* at $\tau = 182$.

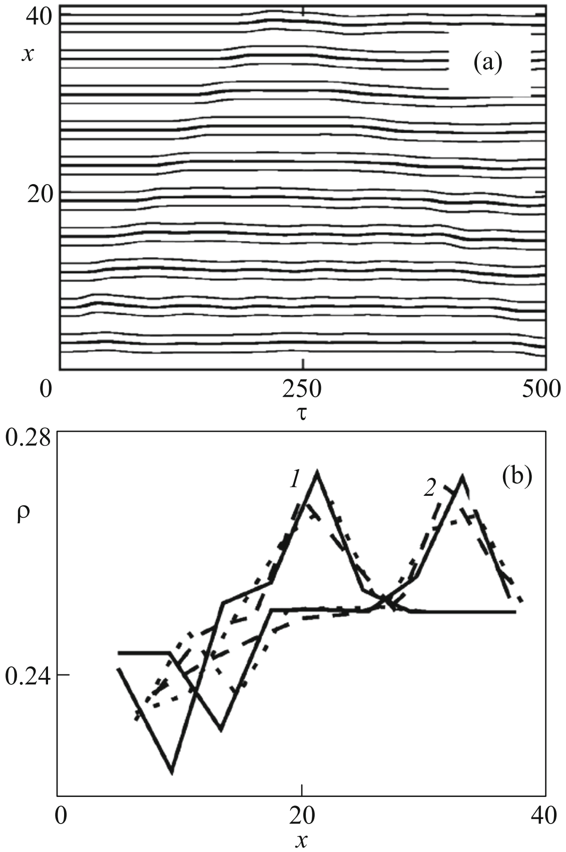

Fig. 6. (a) Time dependences of the displacements of atoms demonstrating the propagation of the gyrosoliton over U and O atoms. (b) Spatial distributions of the microdensity for U demonstrating the displacement of gyrosoliton compression density humps and rarefaction dips from *1* at $\tau = 102$ to *2* at $\tau = 168$.

ted, and dashed lines is the same as in Figs. 4 and 5. The fast gyrosoliton is represented by a high-density compression hump moving at the velocity $v = 0.19$. The slow gyrosoliton is represented by a rarefaction dip moving at the velocity $v = 0.07$. According to Figs. 4 and 6, O atoms contract the distance between the compression and rarefaction gyrosolitons.

The internal structure of the compression gyrosoliton is seen in the detailed video film. Figure 7 shows the dynamics of the internal structure of the compression gyrosoliton on a magnified scale. According to Fig. 7, the highest microdensity at $\tau = 103$ (Fig. 7a), 111 (Fig. 7b), 118 (Fig. 7c), and 126 (Fig. 7d) is reached on the 1D chains *1*, *2*, *3*, and again *1*, respectively, shown in Fig. 2.

Studying the spectrum of vibrations, as well as the phonon spectrum, we took into account only the U–U interaction in the nanocrystal with 126 U atoms. To determine the spectral density $\rho(k, \omega)$, we used the fast Fourier transform procedure. Figure 8 shows this 3D dependence. Branch *1* at a phase velocity of 0.21 spectrally shows the gyrosoliton represented in dynamic dependences at the same velocity. Region *2* of the frequencies $0 < \omega < 0.14$ represents the reduced system of branches of the phonon spectrum shown in Fig. 3. The appearance of high-velocity branch *3* at the velocity $v_3 = 0.63$ is of interest. It can be attributed to gyration.

The velocity of the displacement of an excitation along the helix is higher than the velocity along the axis visually determined from the dynamic dependences, because the length passed over the helix in the time in which the excitation passes along the axis of the nanocrystal is larger. Partial spectra of vibrations of individual chains, as well as phonons, include low-frequency branches with negative dispersion.

It is of interest to study the possibility of diffusion mass transfer of atoms over gyrosolitons similar to the surfing diffusion of light atoms on soliton waves of the sublattice of heavy atoms detected in [5]. We studied the dynamics of the uranium atomic sublattice (Fig. 2), where an impurity atom is located in the longitudinal axis at the initial time. A certain nonstoichiometry was revealed in uranium dioxide samples. An excess O atom was treated as such an impurity atom. In addition to Eqs. (2), the system of equations includes

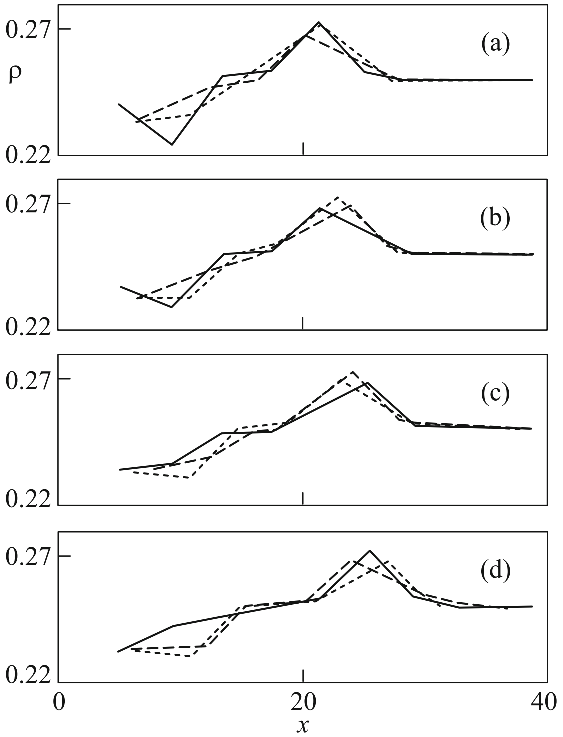

Fig. 7. Spatial distributions of the microdensity in the nanocrystal with U and O atoms demonstrating the motion of the gyrosoliton along the helix. The maxima of the microdensity are located on (a) chain *1* at $\tau = 103$, (b) chain *2* at $\tau = 111$, (c) chain *3* at $\tau = 118$, and (d) chain *1* at $\tau = 126$.

three equations for the coordinates of impurity atoms x_p, y_p, and z_p, the first of which has the form

$$\frac{d^2x_p}{d\tau^2} = \mu\sum_i\left\{\frac{x_p - x_i}{[(x_p-x_i)^2+(y_p-y_i)^2+(z_p-z_i)^2]^7} - \frac{x_p-x_i}{[(x_p-x_i)^2+(y_p-y_i)^2+(z_p-z_i)^2]^4}\right\}, \tag{5}$$

where x_i, y_i, and z_i are the coordinates of U atoms in Fig. 2 and the inverse effect of the light impurity surfer atom on vibrations of the main sublattice of heavy atoms is disregarded as in Eq. (2).

The dynamic dependences of the x coordinates of U and impurity atoms obtained by solving the system of Eqs. (2) and (5) with the initial conditions $x_p = 25$ and the initial velocity of the first U atom $v_0 = 0.4$ is shown in Fig. 9a, where *1* is the gyrosoliton trajectory and *2* is the trajectory of the impurity atom. It is seen that, owing to the interaction with the gyrosoliton, the impurity atom is shifted, following the gyrosoliton, toward large x coordinates. The displacement of the impurity atom following the gyrosoliton is seen in Fig. 9b, where the region of meeting of the gyrosoliton and impurity atom is shown on a magnified scale. The frequency of vibrations of the impurity atom $\omega = 0.3$

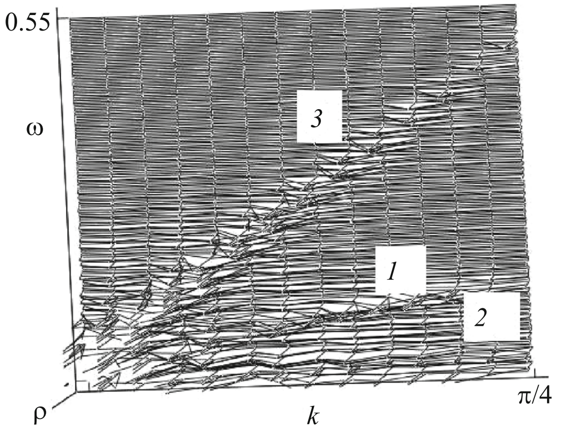

Fig. 8. Three-dimensional spectral density versus the wave vector and frequency demonstrating high-frequency branches *1* and *3* and low-frequency branch *2*.

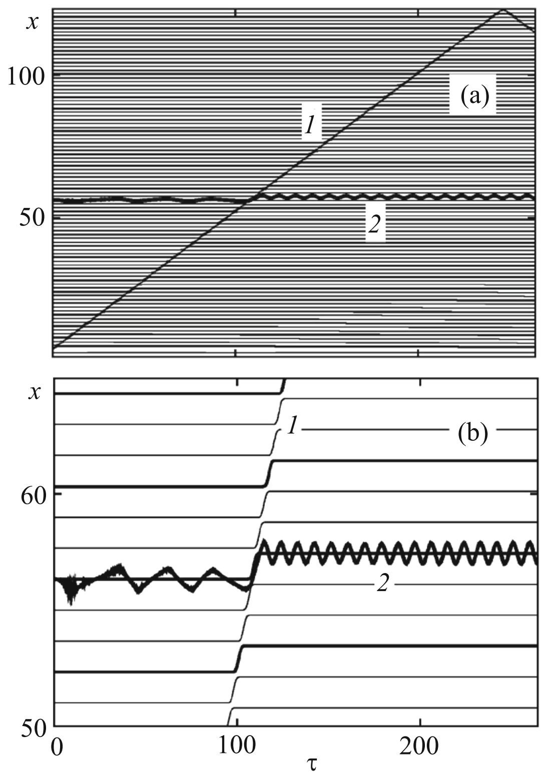

Fig. 9. (a) Time dependences of displacements of atoms of the nanocrystal and impurity atom demonstrating the trajectories of motion of the (*1*) gyrosoliton and (*2*) impurity atom with its intersection. (b) Magnified region of the intersection of the trajectories of the soliton and impurity atom shown in panel (a) demonstrating the entrainment of the impurity atom by the gyrosoliton and an increase in the frequency of vibrations of the impurity atom after their meeting.

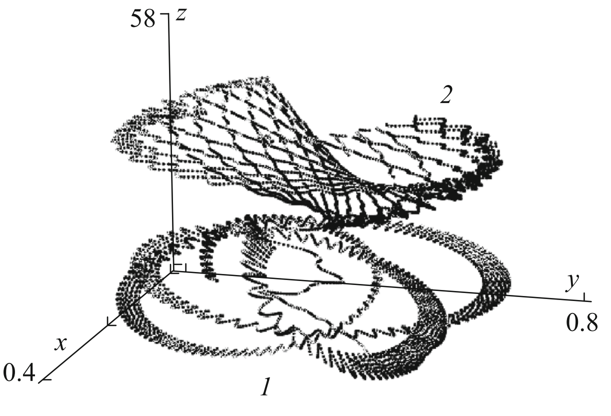

Fig. 10. Three-dimensional representation of the trajectory of motion of the impurity atom inside the nanocrystal: (*1*) region of walks of the impurity atom inside the nanocrystal with the rotation element before meeting with the gyrosoliton and (*2*) trajectory of pronounced rotational motion and entrainment of the impurity atom by the gyrosoliton.

increases after meeting with the gyrosoliton by a factor of 4.

The dynamics of motion of the impurity atom is shown in Fig. 10 in the form of the 3D dependence $x_p = x_p(y_p, z_p)$. The video clip shows that, before meeting with the gyrosoliton, the impurity atom walks with the rotation elements inside the prism shown in Fig. 2 in region *1* in Fig. 10. After meeting with the gyrosoliton, the impurity atom is transferred to the rotation about the *c* axis fixed with the direction of the gyrosoliton with rise at larger *x* coordinates in region *2* in Fig. 10. It was shown in [5] that, at stochastic generation of the energy at one boundary of the crystal and the energy release at the other boundary, because of the interaction of impurity atoms with solitons, impurity atoms are stochastically displaced in different directions (surfing diffusion) with mass transfer in one direction. Figure 10 shows the main dynamic act of the kinetic process of surfing–diffusion of the impurity atom to the gyrosoliton. The stochastic generation of the energy will be accompanied by a sequence of such acts constituting diffusion mass transfer to the gyrosoliton.

It is of interest to analyze the possibility of generation of gyrosolitons in crystal systems of larger dimensions. The hexagon of atoms with the seventh atom at the center shown in Fig. 11 is the element, which is next in magnitude and complexity, of the hexagonal crystal structure of UO_2 with close packing in the plane of the figure. Each unit triangle is the projection of the above prism with 1D UO_2 crystals. The number of atoms in each 1D crystal, $N = 100$, is much larger than that in the previous calculations. The neighboring triangles with one common side have clockwise and counterclockwise directions of helical rotation. Unclosed circles with arrows inside each unit triangle

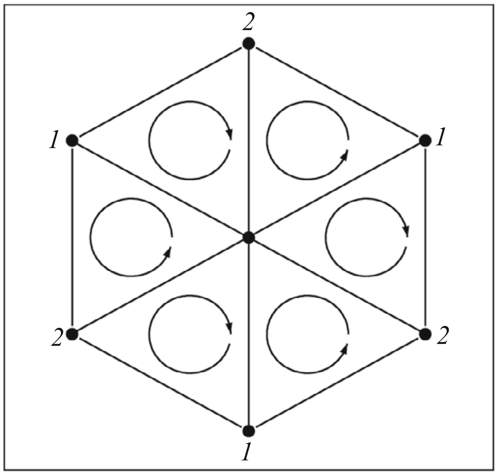

Fig. 11. Gyrosolitons in a group of six nanotubes constituting a hexagonal prism.

specify the directions of such rotation at orthogonal displacement. Digits *1* and *2* conditionally mark prisms with these opposite rotations. It is noteworthy that the directions of rotation coincide with each other on the common sides of two neighboring triangles.

In order to keep symmetry, the initial condition was taken such that the boundary atom of the 1D crystal located at the center of the hexagon in Fig. 11 has the dimensionless velocity $v = 0.6$ at the initial time. The time dependences of displacements of atoms were calculated in the range $0 < \tau < T = 1200$ with the division of T into $M = 1.2 \times 10^5$ intervals. These dependences are shown in Fig. 12. Owing to the symmetry of Fig. 11, the corresponding degeneracy is observed.

Figure 12 indicates that the motion of the primary soliton at the velocity $v = 0.6$ is accompanied by the motion of finite discrete secondary solitons with

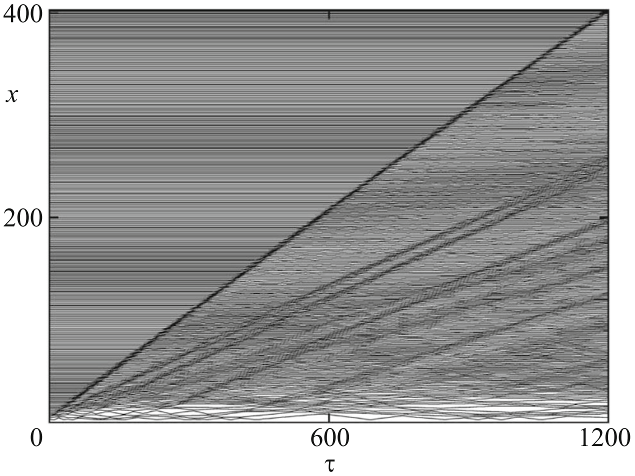

Fig. 12. Time dependences of displacements of atoms in a group of nanotubes constituting a hexagonal prism.

decreasing velocities. As in a smaller crystal, the alternation of maxima of the density on circularly successive 1D crystals was observed for the primary soliton. This indicates the helical motion conditionally indicated by arrows in Fig. 11.

This work was supported jointly by the Russian Foundation for Basic Research and the Government of the Kaluga Region (project no. 14-48-03080).

REFERENCES

1. M. E. Manley, M. Yethirag, H. Sinn, H. M. Volz, A. Alatas, J. C. Lashley, W. L. Hults, G. H. Lander, and J. L. Smith, Phys. Rev. Lett. **96**, 125501 (2006).
2. O. A. Dubovsky and A. V. Orlov, Phys. Solid State **52**, 899 (2010).
3. M. E. Manley, M. L. Abernathy, N. I. Agladze, and A. J. Sievers, Sci. Rep. **1**, 1 (2011).
4. I. S. Kurina, V. V. Popov, and V. N. Kharitonov, At. Energy **101**, 802 (2006).
5. O. A. Dubovsky, V. A. Semenov, A. V. Orlov, and V. V. Sudarev, Phys. Solid State **56**, 1840 (2014).
6. O. A. Dubovsky, V. A. Semenov, A. V. Orlov, and V. V. Sudarev, Phys. Solid State **57**, 1407 (2015).
7. M. Toda, *Theory of Nonlinear Lattices* (Springer, Berlin, 1981).
8. V. M. Agranovich and O. A. Dubovsky, *Optical Properties of Mixed Crystals* (North-Holland, Amsterdam, 1988).
9. V. M. Agranovich, O. A. Dubovsky, and A. V. Orlov, Phys. Lett. A **119**, 83 (1986).
10. V. M. Agranovich, O. A. Dubovsky, and A. V. Orlov, Sov. Phys. Solid State **32**, 1386 (1990).
11. O. A. Dubovsky and A. V. Orlov, Sov. Phys. Solid State **32**, 1397 (1990).
12. R. K. Dodd, J. C. Eilbeck, J. D. Gibbon, and H. C. Morris, *Solitons and Nonlinear Equations* (Academic, New York, 1988).
13. A. I. Kolesnikov, M. Prager, J. Tomkinson, I. O. Bashkin, V. Yu. Malyshev, and E. G. Ponyatovskii, J. Phys.: Condens. Matter **3**, 5927 (1991).
14. O. A. Dubovsky and A. V. Orlov, Phys. Solid State **55**, 1703 (2013).
15. O. A. Dubovsky and A. V. Orlov, JETP Lett. **96**, 461 (2012).
16. O. A. Dubovsky and A. V. Orlov, JETP Lett. **87**, 414 (2008).
17. V. M. Agranovich and V. L. Ginzburg, *Crystal Optics with Spatial Dispersion and Excitons* (Nauka, Moscow, 1965; Springer, Berlin, 1984).
18. V. M. Agranovich and O. A. Dubovsky, JETP Lett. **26**, 488 (1977).
19. V. M. Agranovich and O. A. Dubovsky, Sov. Phys. Solid State **20**, 1867 (1978).
20. O. A. Dubovsky and A. V. Orlov, Phys. Solid State **41**, 302 (1999).
21. O. A. Dubovsky and A. V. Orlov, Crystallogr. Rep. **56**, 42 (2011).

Translated by R. Tyapaev